IEEE ROBOTICS & AUTOMATION LETTERS
A PUBLICATION OF THE IEEE ROBOTICS & AUTOMATION SOCIETY

IEEE Xplore® Digital Library
http://ieeexplore.ieee.org/Xplore

Soft haptic device to render the sensation of flying like a drone

Carine Rognon[1], *Student Member, IEEE*, Margaret Koehler[2], *Student Member, IEEE*, Christian Duriez[3], *Member, IEEE*, Dario Floreano[1], *Senior Member, IEEE*, and Allison M. Okamura[2], *Fellow, IEEE*

***Abstract*—Haptic feedback located on the torso is proposed to enhance the state awareness of a user in virtual reality or during teleoperation while leaving the hands free for manipulation and communication. We provide haptic feedback on the torso by compressing a set of closed air pouches against the skin in order to render the sensation of air pressure when piloting a drone. The pouch devices are cable-driven and integrated in a wearable soft exoskeleton, called the FlyJacket. A mechanical model and simulation of a pouch device were developed in order to determine appropriate parameters, including the air pouch inner pressure, its attachment point, and the cable position. Using the simulation results, a set of pouch devices were constructed and integrated into the soft exoskeleton on both sides of the upper chest and middle of the back. The mechanical performance of the constructed device is close to that predicted by the simulation. Application of the haptic device in a flight task in which the user controls a drone using upper body movements was demonstrated with a user study. Adding haptic feedback during a stabilization task reduced the user's workload and improved the state awareness of the user.**

***Index Terms*—Soft Robot Applications; Haptics and Haptic Interfaces; Wearable Robots**

I. Introduction

HAPTIC devices that provide touch feedback to the fingers and hands have proven to be a compelling way of transmitting information and enhancing training and performance of a variety of tasks. However, many applications require the hands to be available for manipulation or interaction. This motivates the study of haptic feedback to other parts of the body, such as the arms and torso, with a focus on tactile feedback (stimulation of the skin). Another potential benefit of haptic feedback located on parts of the body other than the fingers and hands is that it could increase state awareness of the user in a virtual or teleoperated task in which relevant sensations should occur on those parts of the body. For example, it has been shown that immersion in a virtual world can be improved with a tactile feedback vest using vibrations [1], [2] and pneumatic actuators [3].

Our work involves tactile feedback on the upper body in order to enhance realism and increase the flight awareness of the user during teleoperation of a flying drone robot. In prior work, vibrotactile vests have been used to communicate information to pilots, e.g. [4]. Tactile feedback on the torso has also been used to connect between humans located remotely from each other [5], [6], [7] and enhance emotions [8], [9]. Various actuators have been used to achieve tactile feedback on the torso. Shape memory alloy actuators [10] and vibrotactile actuators [11] have been used for navigation tasks. Pneumatic actuators located on the torso [12] and vibrators located on the limbs were used in rehabilitation [13], [14], as well as for motor learning tasks [15]. Products dedicated for gaming have also used pneumatics (e.g. Tactsuit from bHaptics Inc., Daejeon, Republic of Korea) and vibration (e.g. TN game vest from Phantomsense, WA, USA). A whole-body haptic system used blowing air to create the sensation of navigating a windy environment [16].

To enhance human teleoperation of a drone, researchers have identified patterns of natural and intuitive body movements that can be used to control a drone [17]. People use the inclination of their torso with their arms spread out to control the drone. Accordingly, an upper body soft exoskeleton, called FlyJacket, was developed to record the body movements and transmit the commands to the drone [18]. This exoskeleton includes passive arm supports to prevent fatigue during the flight. In this previous work, the user received only visual feedback about the drone maneuvers.

We propose that, in order to enhance flight awareness, sensations of the air pressure during drone movements could provide valuable feedback to help the user perceive the drone state. A tactile feedback device, rather than a kinesthetic device, would facilitate wearability and portability. In most prior work, tactile feedback was provided using vibrotactile actuators. These have the advantage of being small and lightweight, which makes them easy to integrate into wearable devices. However, the vibration sensation cannot realistically transmit the sensation of skin compression as is required to recreate the air pressure felt by the drone. Another approach is using active pneumatics. Such device could transmit compressive force normal to the skin. However, pneumatic actuation requires valves and an air source, which is currently cumbersome and complex to

Manuscript received: October 15, 2018; Revised February 10, 2019; Accepted March 10, 2019.

This paper was recommended for publication by Editor Kyu-Jin Cho upon evaluation of the Associate Editor and Reviewers' comments. This work was supported by the Swiss National Science Foundation (SNSF) through the National Centre of Competence in Research Robotics (NCCR Robotics) and through the FLAG-ERA project RoboCom++, the SNSF Mobility program, and the U.S. National Science Foundation grant 1830163.

[1]C. Rognon and D. Floreano are with the Laboratory of Intelligent Systems, Ecole Polytechnique Federale de Lausanne, Lausanne 1015, Switzerland carine.rognon@epfl.ch, dario.floreano@epfl.ch

[2]M. Koehler and A.M. Okamura are with the Department of Mechanical Engineering, Stanford University, Stanford, CA 94305 USA mkoehler@stanford.edu, aokamura@stanford.edu

[3]C. Duriez is with INRIA, Defrost Team, and the University of Lille, France christian.duriez@inria.fr

Digital Object Identifier (DOI): see top of this page.

Digital Object Identifier 10.1109/LRA.2019.2907432

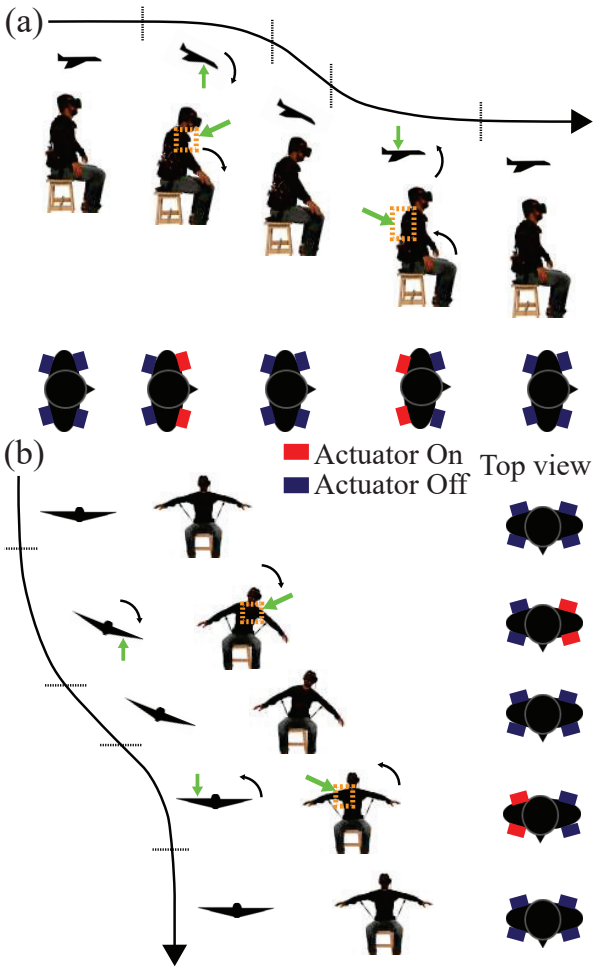

Fig. 1: Forces rendered on the torso relating to the drone orientation and schema of the actuated tactile devices. The actuated devices are highlighted in red on the top view of the user. a) During pitch maneuvers. b) During roll maneuvers.

integrate in a portable system. Our device combines the advantages of a soft device that is conformable and safe to interface with the human body, while being actuated by motors in order to be responsive and portable.

The FlyJacket aims to be used for drone rescue missions or inspection and therefore should be portable for easy use in the field. Here, we present a novel approach to render tactile feedback on the torso in order to improve the control of a drone and increase the flight awareness. The developed device gives cues on the drone orientation by rendering air pressure on the torso proportional the centripetal acceleration of the drone via a soft air pouch pressed against the skin. The forces rendered on the user are shown in Fig. 1(a) for pitch maneuvers and in Fig. 1(b) for roll maneuvers.

II. Device Design

To render the sensation of distributed pressure against the body, we developed a tactile device composed of soft, closed air pouches that are compressed against the skin by cables driven by electric motors (Fig. 2).

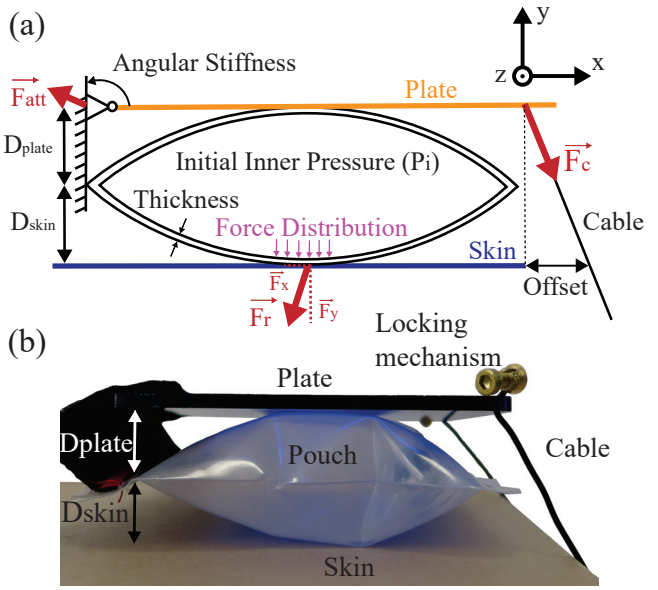

Fig. 2: Tactile device. (a) Analytical model of the soft air-filled pouch being compressed by the plate onto the skin. (b) Image of the mechanism.

The portable actuation via motors is less cumbersome than a pneumatically actuated device. The inner pressure of the pouch can be varied for different applications using more or less inflation, which gives this technique an advantage over other soft material approaches such as foam. In addition, pouches can be deflated during transportation to gain space. Furthermore, the holding structure, in this case the soft exoskeleton, does not need to be tightly attached to the body; the cables allow a large range of motion to generate compression. In order to make the compression of the pouch against the skin relatively uniform, the cables do not pull directly on a pouch's corner or edge, but rather on a rigid plate situated on top of it as shown in Fig. 2. If the cables were directly attached to the pouch, the pouch would deform, and the force transmission efficiency would decrease. One end of both the pouch and the plate are attached to the exoskeleton, and on the other end the plate is attached to the cables.

In order to design the force transmission from the actuator to the skin and make the sensation as realistic as possible, two output variables are considered: the force vector (magnitude and direction), and the pressure distribution. First, we optimize the change in the force vector that occurs between the uncompressed and compressed state. The aim is to effectively minimize the motor torque and limit losses on the exoskeleton, to avoid applying unnecessary reaction forces to other parts of the body. The direction of the force is an important component. Force in the y direction (according to Fig. 2) applies normal pressure on the skin, triggering Merkel mechanoreceptors [19]. Forces in x and z directions induce shear forces, which trigger Ruffini mechanoreceptors. Stimulating multiple types of mechanoreceptors raises the awareness of the user. The force magnitude and pressure distribution are related; humans are sensitive to magnitudes of forces as well as the contact area [20]. Ideally, no pressure should be applied by the pouch

on the skin before compression, and the area in contact with the skin once the pouch is fully compressed should be as large as possible to have the largest spreading possible and therefore maximizing the change of sensations.

III. Modeling and Simulation

A. Model and Simulation Procedure

In order to study the influence of the tactile device parameters on both outputs (the force vector and the pressure distribution) and determine the best parameters, a simulation of the device was implemented using SOFA (Simulation Open Framework Architecture) software [21] as shown in Fig. 3.

The pouch is represented by two rectangular thin shells sealed together at the four sides. These two layers are defined by a mesh of 10×8 triangles (Fig. 3(a)). The number of triangles for the mesh was chosen as a compromise between precision and simulation duration. Refining the mesh further did not substantially change the results, while greatly increasing the time required for each simulation.

The pouch is attached on one side to a rigid fixation point. The distance between the pouch fixation and the skin is D_{skin} (see Fig. 3(b)); this represents how closely the jacket is tightened to the body. The skin is represented by a non-deformable and flat plane. It consists of two gridded planes: a reference plane that does not move and a second plane of very high stiffness ($10^5 \frac{N}{m}$). The small displacements between these two planes, due to the force applied by the pouch, are used to calculate the force on each grid element. The upper plate used to compress the pouch is also non-deformable and attached at a distance D_{plate} from the fixation point of the pouch. Opposite these attachment points, two cables, one attached at each corner, pull on the plate. The interaction between the upper plate and the pouch and the skin and the pouch is modeled as Coulomb friction with μ = 0.5.

At the start of the simulation, the pouch is inflated to an initial inner pressure with no force on the cables. For the remainder of the simulation, the amount of air in the pouch remains constant, and the pressure in the pouch depends on the volume of the pouch according to Boyle's law (i.e., the product of pressure and volume remains constant). The compression of the pouch is simulated as a cycle that starts from no force (0 N) on the cables, increases gradually to 14 N, and then decreases to 0 N at the same rate. The cables pull from a fixed pull point, which is assumed to be the location of the cable routing on the jacket. The forces on the skin in x, y, and z directions are recorded during the simulation. The pressure distribution on the skin is recorded using the normal force on each element of the grid divided by its area.

B. Simulation Parameters and Results

The parameters are described in Table I, and the effects of varying these parameters on simulation results are shown in Fig. 4. The parameters were varied independently, and the resulting force vectors and pressure distributions were obtained using the simulation in SOFA. Parameters were tested in a range of value that were physically possible to be used when building the hardware. The simulation was done

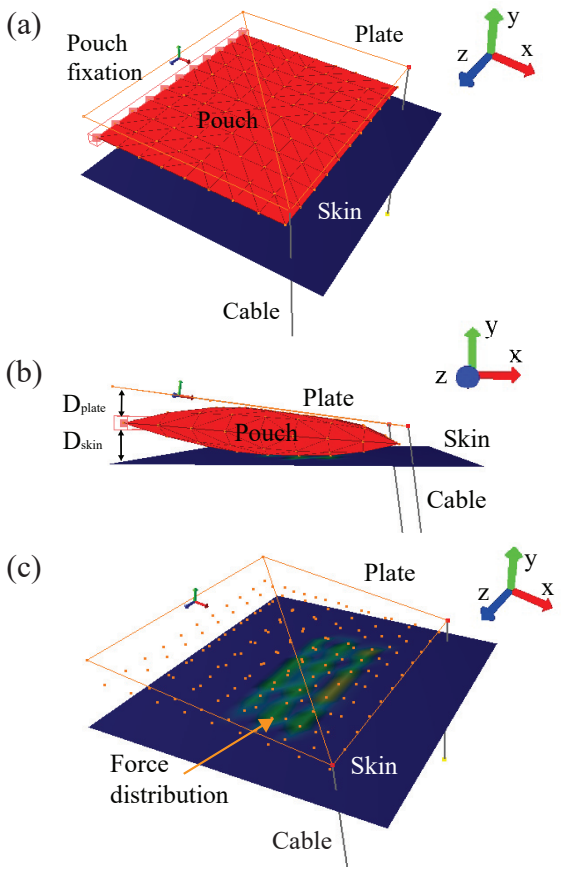

Fig. 3: Simulation of the air pouch being compressed against the skin by a plate, using SOFA software. (a) Top perspective view of the pouch, with the triangular meshing of the pouch (in red). (b) Side view of the inflated air pouch (in red) being compressed by the plate. (c) Top perspective view of the force distribution on the skin during compression. Only the meshing points of the pouch are visible (orange dots) to enable visualization.

TABLE I: Parameters of the air pouch

Parameters	Range tested	Device parameters
Thickness (m)	0.0005 - 0.005	0.0005
Young modulus (GPa)	0.05 - 4	0.3
Initial Inner Pressure, P_i (kPa)	1 - 10	6
Angular Stiffness, AS ($\frac{Nm}{rad}$)	0.5 - 10.5	2
Cable offset in X (m)	0 - 0.32	0
Cable offset in Z (m)	0 - 0.2	0
D_{skin} (m)	0.005 - 0.021	0.0011
D_{plate} (m)	0.002 - 0.018	0.01

quasi-statically, so dynamic forces are not reflected in the results. The physical characteristics of the pouch – the Young's modulus of the material and the thickness – where also tested but did not have a major influence on either the force vector or the pressure distribution, for a realistic range of parameters.

The plate can be thought of as a lever. The torque applied by the cables is balanced predominately by the pressure of the pouch but also by the small angular stiffness at the attachment point. The distribution of contact of the pouch on the plate, which is influenced by the pouch internal pressure and the mounting distances, D_{skin} and D_{plate}, determines

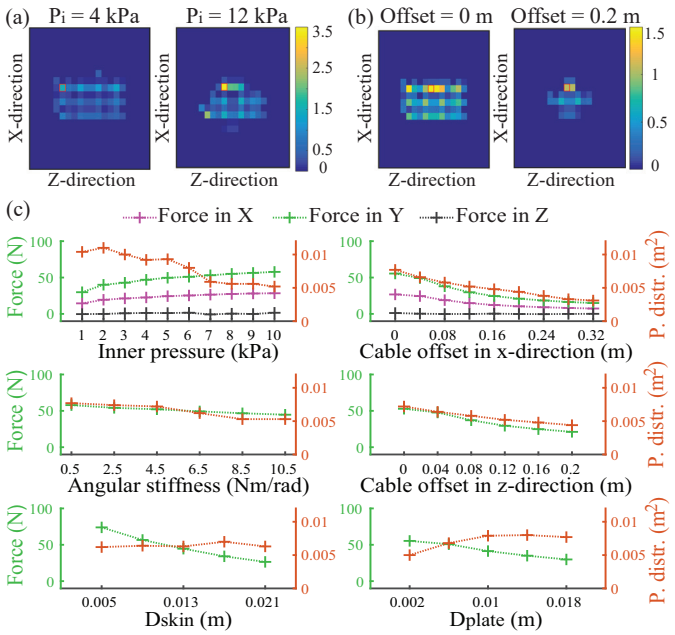

Fig. 4: Results of parameter variation in simulation. (a) Pressure distribution (kPa) normal to the skin (in y direction) at maximum cable force for an inner pressure (P_i) of 4 kPa (left) and 12 kPa (right). (b) Pressure distribution (kPa) normal to the skin (in y direction) at maximum cable force for no cable offset (left) and 0.2 m offset in x direction (right). (c) Influence on the two outputs (force in y and pressure distribution) when varying each device parameters over their tested range. The first two graphs include the force component in x and z.

the effective radius of the force and contact area between the pouch and the plate. Given a particular cable force, the torque on the plate from the cables and therefore the reaction force required from the pouch, is maximized when the cables are perpendicular to the plate. All of these variables influence the force vector and pressure distribution on the skin.

The initial inner pressure of the pouch P_i influences both the resulting force and the pressure distribution (Fig. 4(a) and (c)). When the initial inner pressure increases, the amount of air in the pouch increases, leading to different contact conditions between the pouch and the plate, as well as between the pouch and the skin. The torque applied by the cables is the same for these tests, but the change in contact conditions results in different force distributions on the skin. As the pouch internal pressure increases, the force applied to the skin increases (Fig. 4(c)). On the other hand, as the initial inner pressure increases, the pressure distribution decreases; less of the surface of the pouch is in contact with the skin (Fig. 4(a)) but the maximum pressure on one cell increases; the pressure is less distributed. Depending on the application and the desired tactile sensations, more weight can be given to the resulting force or the pressure distribution by varying this initial inner pressure.

The angular stiffness of the plate should be as small as possible in order to have the force produced by the cables be used to compress the pouch and not to rotate the plate. Both the resulting force and the pressure distribution decrease when the angular stiffness of the plate increases.

As in the case of increasing the initial inner pressure, both distances – between the pouch and the skin (D_{skin}) and the plate (D_{plate}) – have a trade-off between the resulting force and the pressure distribution; the force decreases when the distance increases (when the jacket is less tightly attached to the body) but the change in pressure distribution increases. These three parameters (P_i, D_{skin} and D_{plate}) can be set according to the desired sensations.

The offsets of the cables in the x and z directions influence the resulting force and the pressure distribution (Fig. 4(a) and (b)). As the cables become more perpendicular to the top plate, more force is transmitted to the pouch because less force is lost to reaction forces from the fixation point of the plate. Angling the cables away from the perpendicular does not greatly increase the shear force (x and z directions), but it does decrease the normal force substantially, which is more critical to our application. Nevertheless, the current configuration already gives a substantial shear force in x direction because the compression of the plate is not vertical, but rather is done by rotating the plate.

IV. Hardware

A. Implementation

The aim of the haptic device is to render the sensation of the centripetal acceleration of the drone to the FlyJacket user. Therefore, in order to give compressive forces on the torso when “pitching up”, “pitching down”, “rolling left”, and “rolling right”, four pouches are included in the soft exoskeleton.

The dimensions of the pouch need to be as large as possible in order to have the largest surface in contact with the body. However, this characteristic is limited by the space available in the soft exoskeleton. Pouches were located on the torso so that the haptic feedback was collocated with the point of actuation on the user’s body. They were placed on the upper torso as these parts remain more stable during torso movements compared to the lower part of the torso. Four pouches were used, as this is the minimal number which can render the sensation in all the flight directions. More pouches could give finer sensations, but would also increase the complexity and the weight of the device. Looking at the results of the user study (see Sec. V), the pouch is sufficiently large (100 mm $\times$ 80 mm) to be clearly perceived by the user and transmit a noticeable sensation.

Two pouches are placed on the front part of the jacket (Figs. 5(a) and 5(c)). They are located on each side of the upper chest with the cables pulling against the torso to give the sensation of being compressed when the drone is pitching down. The other two pouches are placed on each side of the back as shown in Fig. 5(b) and highlighted in Fig. 5(d) to give the sensation of being pushed forward when the drone is pitching up.

Using the simulation results to inform the design, the following parameters for the device were selected and are summarized in Table I. The pouch is made of low-density

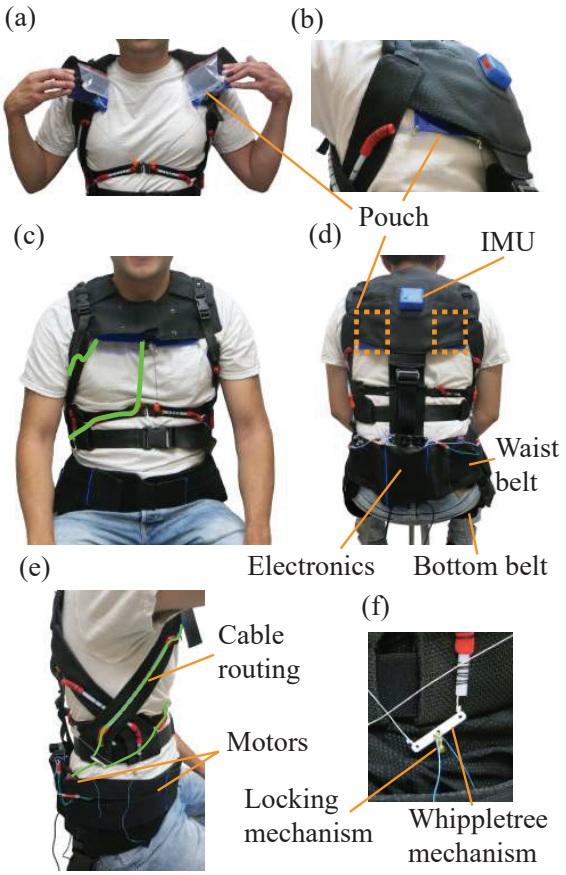

Fig. 5: Hardware implementation of the device in the FlyJacket (a) View of the front pouches. (b) View of the left back pouch. (c) Front view of the device. The cables of the left side are highlighted in green. (d) Back view of the device highlighting the pouch placement. (e) Side view highlighting the front cable routing in green. (f) Whippletree mechanism to distribute the tension equally on both cables, and the locking mechanism.

polyethylene (LDPE) with a thickness of 0.5 mm and a Young's Modulus of 0.3 GPa, and it can be inflated and deflated easily via tubing closed with a removable cap. The compressive plate is made of acrylic in order to be both rigid and lightweight, and it has the same dimensions as the pouch. Both the pouch and the plate are connected to the soft exoskeleton with a piece of fabric (Fig. 2(b)), which provides a low angular stiffness (2 $\frac{Nm}{rad}$) at the fixation point of the plate.

In cases where the force and pressure distribution response were the same with the variation of the parameter (such as cable offset in the x and z directions and the angular stiffness of the plate), the parameter was made small as possible within feasible manufacturing constraints. In other cases, the tradeoff between force and pressure distribution, as well as the manufacturing, was considered. An inner pressure of 6 kPa was used as a compromise between high force and large pressure distribution. D_{skin} and D_{plate} were also set in the middle of the tested range, to 0.0011 m and 0.01 m respectively, for the same reason. The cables should be oriented as perpendicular to the skin as possible to optimize the force transmission. However, as the cable cannot go through the torso, a perfectly perpendicular angle is not possible. Adding an extra band of material to the exoskeleton and a pulley below the pouch was tested as a way to achieve a more perpendicular angle, but due to the compliance of the textile, the pulley was pulled upwards toward the plate and off the skin, rather than pulling the plate down and applying force to the user. Thus, this modification did not show significant improvement for the force transmission. Instead, a wedge can be inserted between the compressive plate and the pouch in order to decrease the angle of the cable pulling on the plate and therefore increase the force applied on the skin (Fig. 6(c)). The angle of the wedge influences proportionally the output force. An angle of 20 degrees was chosen for the hardware measurement as a proof of concept. The wedge is made of 3D-printed Polylactic Acid (PLA) plastic of the same dimension then the pouch and the acrylic plate.

In order to apply forces on the torso in the directions described in Fig. 1, the four electrical motors (DC22S, gear ratio 6.6:1, Maxon Motor, Switzerland) that pull on the cables are placed on the waist belt of the exoskeleton (Fig. 5(d)). The cables, made of Dyneema (diameter 0.4mm, Spiderwire, SC, USA), are routed along the structure of the soft exoskeleton through Polytetrafluoroethylene (PTFE) tubes in order to limit losses due to friction (Fig. 5(e)). The four motors can be actuated separately, and the control is performed by an Arduino Mega 2560 (Arduino, Italy) with a shield including two double H-bridge drivers (DRV8412, Texas Instruments, TX, USA) located in a pocket on the lower back of the exoskeleton (Fig. 5(d)). In order to prevent the belt from moving when the motors pull on the cables, an extra bottom belt, passing under the person, was added to the exoskeleton. Because only one motor pulls on both cables connected to each compressive plate, a whippletree mechanism was inserted between the output of the motor and the separation of the cables on their routing tubes (see Fig. 5(f)). This mechanism is used to distribute equal tension on the two cables.

A locking mechanism made of a screw and a bolt was used to quickly change the nominal length of the cables to adapt the device between different users' morphologies. It is placed at the end of each cable on the plate (see Fig. 2(b)) and on the whippletree mechanism (Fig. 5(f)).

B. Comparison with Simulation

In order to compare the performance of the hardware device to the results found from simulation, the compression force on the skin (the pressure distribution and the maximum pressure) were measured by placing a capacitive pressure sensor array (Conformable TactArray, Pressure Profile Systems, Los Angeles, CA, USA) between the pouch and the skin as shown in Fig. 6. The pressure sensor is made of an array of 8 $\times$ 6 pressure cells of 25.4 mm $\times$ 25.4 mm. The resulting pressure values were recorded with Pressure Profile System's Chameleon visualization software with a resolution of 0.0276 ± 0.0069 kPa and a scan rate of 20 Hz. The resulting force was calculated by multiplying the recorded pressure by the area of the cell and summing the values of all the cells.

Only the normal force (in the y direction) is measured with this pressure sensor array.

A force sensor (ELFS-T3E-25N, Entran Sensors and Electronics, NJ, USA) was placed in series with the cable in order to measure the applied force (Fig. 6(d)) at a rate of 100 Hz. During the test, the cable was pulled gradually until the force on the cable reached 15 N and then released (this explains the non-symmetric profile of Fig. 7(b) in comparison to the results of the simulation (Fig. 7(a))). Recorded forces were low-pass filtered using a Butterworth filter with a cut-off frequency of 10 Hz. Fig. 7(b) shows the effect of the filtering. Four comparison tests were done: (1), using the device parameters displayed in Table I, (2,3) when lowering the initial internal pressure of the pouch to 1 kPa and then increasing it to 20 kPa in order to investigate the effect of the change of the initial inner pressure, and (4) adding a wedge of 20 degrees between the pouch and the plate. The wedge makes the cables more perpendicular to the plate within the physical constraints of the jacket. The tests were performed on a plastic mannequin as shown in Fig. 6 to avoid the variability between individuals.

Results for the four experiments are listed in Table II, and the data recorded for the device parameters condition are shown in Fig. 7. For the normal device parameters, the mean maximum normal force output is over 20N. The measurements with the hardware are close to the results of the simulation for the four tests; the force in y direction and the maximum pressure in a cell increase both when the initial inner pressure of the pouch increases and with the addition of a wedge between the pouch and the plate. The maximum pressure in a cell is slightly higher in simulation than for the measurement with the hardware. This can be due to the alignment between the surface of the pouch and the cells in the pressure sensing array. With the hardware measurement, the pouch was likely located in between three columns of cells instead of the two used in the simulation. This effect can be seen when comparing the pressure distribution between Figs. 7(c) and 7(d). The pressure distribution is similar between the simulation (Fig. 7(c)) and the hardware measurement (Fig. 7(d)). However, it is difficult to quantify because of the lower resolution of the pressure sensor array – only 4×4 instead of 20×20 in the previous results of the simulation (Fig. 4).

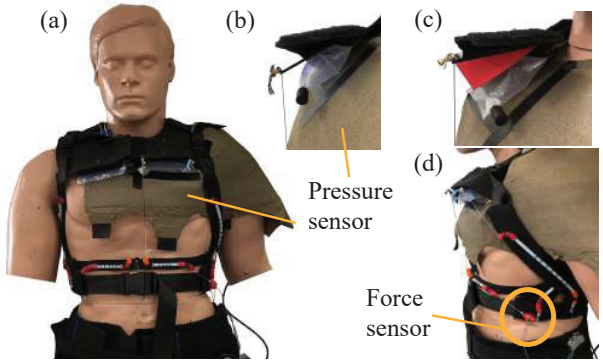

Fig. 6: Testing setup to measure the force transmitted by the hardware on the skin using a mannequin. (a) Front view. (b) Close up view of the pouch. (c) Close up view of the pouch with the wedge. (d) Side view highlighting the force sensor.

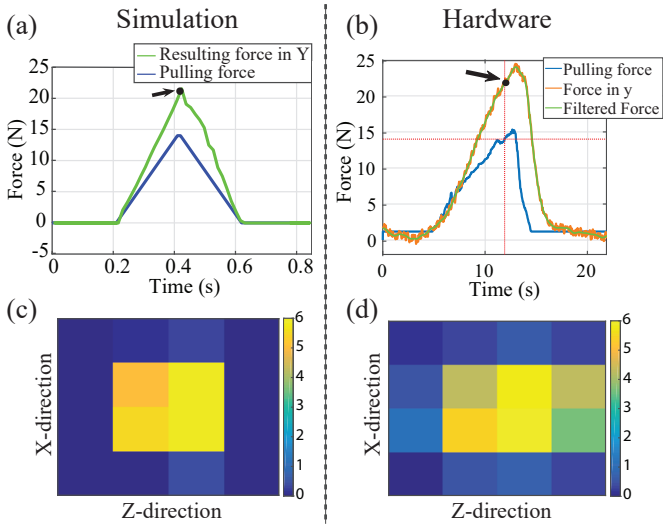

Fig. 7: Comparison of the forces and pressures transmitted to the skin between the simulation and the hardware, with a force of 14 N pulling on the cables. (a) Resulting force (N) in y direction in simulation. The simulation is quasi-static so its rate is not significant. (b) The evolution of the resulting force (N) in y direction measured with the hardware. The resulting force is dependent on the applied pulling force, and the arrow points to the data at a compression of 14 N.

(c) Pressure distribution (kPa) normal to the skin in simulation. (d) Pressure distribution (kPa) measured with the hardware. (·) denotes the value of the force at 14 N.

V. Application in a Virtual Flight Task

A. Methods

The effectiveness of the haptic device was evaluated in a task in which users stabilized a simulated fixed-wing drone following a perturbation. The aim of this study is to investigate how the haptic feedback can improve the user's awareness of the drone attitude and whether it can reduce the workload of the user during flight. Twelve participants took part in the study (four women and eight men, age 27 $\pm$ 4.9 years; mean $\pm$ SD). They flew in a flight simulator developed in Unity3D (Unity Technologies, San Francisco, CA, USA). The simulator is similar to the one used for previous experiments on drone teleoperation [18]. Participants started with two sessions of free flight of one minute and 30 seconds each, once with tactile feedback and once without. The goal of these sessions was to familiarize participants with the flight setup and the tactile feedback.

Then, they had to perform two sessions of stabilizing the drone after perturbations in roll (i.e. from the side). One session was performed with the tactile feedback, and the other session without. The order of these two sessions was pseudo-randomized among participants. A cross in the middle of the field of view indicated the drone's attitude (Fig. 8(a)). Each session was composed of 36 perturbations in which the roll angle of the drone was shifted by -30, -20, -10, 10, 20 or 30 degrees (a negative angle corresponds to a counter-clockwise

TABLE II: Comparison Between Simulation and Hardware Measurements

	Maximum Normal Force in Simulation (N)	Maximum Normal Force of the Hardware (N) (mean ± std)	Maximum Pressure in Simulation (kPa)	Maximum Pressure of the Hardware (kPa) (mean ± std)
Normal	20.82	20.29 ± 2.11	7.1	5.78 ± 0.52
Initial Inner Pressure: 1 kPa	4.12	4.10 ± 0.88	1.89	0.92 ± 0.20
Initial Inner Pressure: 20 kPa	39.86	37.18 ± 1.62	13.65	14.85± 0.52
Wedge	31.01	34.10 ± 4.92	9.77	9.17 ± 0.65

roll and a positive to a clockwise roll). After each perturbation, the participants had to re-align the cross with the horizon as fast as possible (Fig. 8(b)). An example of perturbation is shown in Fig. 8(c)). Most of the time, due to its slow dynamics, the drone did not reach the whole shift of roll angle because the user reaction to straighten the position was faster than the drone to reach its new commanded angle. The perturbations were pseudo-randomly ordered and separated by either seven, eight, nine or ten seconds. During these tasks, participants had control on only the roll of the plane by bending their torso laterally. Participants were free to move their torso in any direction, but other movements had no influence on the the drone. The torso movements were recorded with an inertial measurement unit (Xsens, Enschede, The Netherlands) located on the torso and transformed into drone commands.

They received tactile feedback through the device recreating the drone centripetal acceleration (Fig. 1), where the desired force is related to the drone motion as follows:

$$F = ma = m\frac{v^2}{R} = mv\omega \tag{1}$$

In the simulator, the mass of the drone (m) and its forward speed (v) are constant. The force varies with the angular velocity of the drone (ω). To simplify the information the user receives, the aerodynamic forces of the drone (drag, lift, external disturbances, etc.) were not recreated. During maneuvers, the force applied by the tactile device is proportional to the angular velocity of the drone. The relationship between angular velocity and the force rendered during the flight is given by Eq. 2.

$$F = 2 \cdot \sqrt{|\omega|} + 2 \tag{2}$$

The force is proportional to the square root of the angular velocity to intensify the force for small angular velocities. The purpose of the offset (2 N) is to always keep some tension in the cable to prevent slack. The maximal angular velocity (± 15 deg/s) corresponds to a force slightly lower than 10 N. The actuator can produce a higher force but it was found uncomfortable during preliminary experiments. The roll angle of the simulated drone was recorded. Stability criteria were to maintain the roll angle within a stabilization zone defined as a range of -3 to 3 degrees, which corresponds to the static noise of the IMU, for a stability period of three seconds (Fig. 8(c)). The stabilization time (the time between the perturbation and the end of the stability period) and the number of overshoots (defined as crossing outside the stabilization zone) were computed.

At the end of each task, participants completed a NASA-TLX questionnaire, in which participants had to assess the workload for the two flight stabilization tasks on a scale from 1 to 100. Workload is composed of six components: physical demand, mental demand, effort, temporal demand, frustration, and performance. For stabilization time, overshoot, and workload metrics, on a per participant basis, relative results were computed as the results from the task with feedback subtracted from the results from the task without feedback. Therefore, a positive relative result signifies an improvement in the task with tactile feedback.

B. Results

While the stabilization time was not influenced by the haptic feedback (-0.17 ± 0.39 seconds), the absence of haptic feedback led to slightly larger number of control overshoots (2.33 ± 3.94 more overshoots, p = 0.065). As shown in Fig.8(d), there is no difference in the overall workload between the two tasks, but some of the components of workload are reduced with haptic feedback. Statistically significant differences (based on a t-test) were found for the relative mental workload (p = 0.0112), physical workload (p = 0.0356) and temporal workload (p = 0.0132). There is no statistical difference for the other contributions (effort, frustration, and performance). Participants reported that it was easier to know how to stabilize the drone – in which direction and with what intensity – and that the haptic feedback was a good complement to the visual feedback.

VI. Conclusion

The presented haptic feedback device addresses the challenges of rendering forces relative to the centripetal acceleration of a drone on the torso of a human teleoperator, while maintaining compliance and portability. Its parameters were studied with a simulated model of the device. The hardware built based on the results of the simulation showed performance close to the simulation. Also, the construction of the device is simple and its components are inexpensive, which makes this tactile feedback device widely accessible. The tactile device was assessed on twelve participants who performed a virtual drone stabilization task. The tactile feedback increased the state awareness of the user by giving them information about the direction and intensity of the perturbation while reducing their mental, physical and temporal workload.

Some improvements can be made in future work. The aerodynamic forces (lift, drag, external disturbances such as wind gusts, etc.) could be implemented with the same hardware by changing the actuator control. It would be interesting to test if users can still understand the tactile cues in this more complex scenario. More actuators can also be implemented into the soft exoskeleton to render more complex sensations such as force propagation along the torso. Additional work could explore a

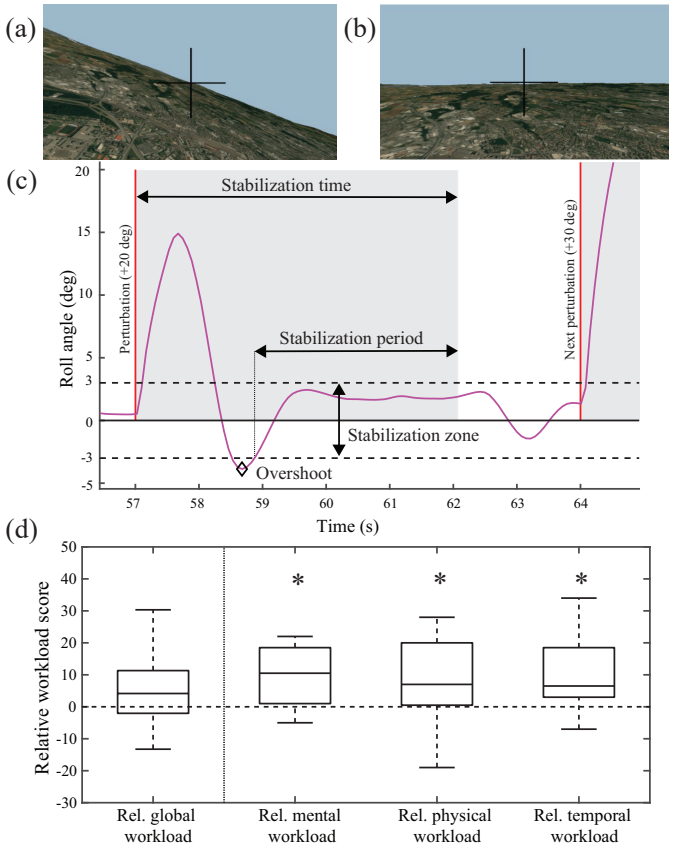

Fig. 8: Application to a flight task. (a) Environment after a perturbation of 30 degrees. (b) Environment stabilized. (c) Example of the drone roll angle for a perturbation of 20 deg with feedback (Participant 7). (d) Results of the workload questionnaire, where the relative score is the difference between the score with haptic feedback and the score without haptic feedback. Asterisks (*) denote $p < 0.05$.

change in the texture of the pouch surface. Indeed, changing the friction coefficient between the pouch and the skin could produce other types of sensations.

The next step of the project will be to perform quantitative experiments with a larger number of participants in order to assess the feedback accuracy, the time to recognize cues, the influence on flight performance, and a quantitative measurement of the sense of realism.

Due to its simplicity, this tactile feedback approach can be used for many different applications such as the teleoperation of underwater robots, the transmission of emotion between remote humans, and for gaming applications.

ACKNOWLEDGMENTS

The authors would like to acknowledge S. Frishman for his valuable help with the hardware.

REFERENCES

[1] U. Yang, Y. Jang, and G. J. Kim, "Designing a vibro-tactile wear for close range interaction for vr-based motion training," in *International Conference on Artificial Reality and Telexistence*, 2002, pp. 4–9.

[2] R. W. Lindeman, R. Page, Y. Yanagida, and J. L. Sibert, "Towards full-body haptic feedback: the design and deployment of a spatialized vibrotactile feedback system," in *Proceedings of the ACM symposium on Virtual Reality Software and Technology*, 2004, pp. 146–149.

[3] A. Delazio, K. Nakagaki, R. L. Klatzky, S. E. Hudson, J. F. Lehman, and A. P. Sample, "Force jacket: Pneumatically-actuated jacket for embodied haptic experiences," in *Proc. CHI Conference on Human Factors in Computing Systems*, 2018, p. 320.

[4] W. Karlen, S. Cardin, D. Thalmann, and D. Floreano, "Enhancing pilot performance with a SymBodic system," in *Annual International Conference of the IEEE Engineering in Medicine and Biology Society (EMBC)*, 2010, pp. 6599–6602.

[5] J. K. S. Teh, A. D. Cheok, R. L. Peiris, Y. Choi, V. Thuong, and S. Lai, "Huggy pajama: a mobile parent and child hugging communication system," in *Proceedings of the 7th international conference on Interaction Design and Children*, 2008, pp. 250–257.

[6] J. Cha, M. Eid, L. Rahal, and A. El Saddik, "Hugme: An interpersonal haptic communication system," in *IEEE International Workshop on Haptic Audio Visual Environments and Games*, 2008, pp. 99–102.

[7] D. Tsetserukou, "Haptihug: A novel haptic display for communication of hug over a distance," in *International Conference on Human Haptic Sensing and Touch Enabled Computer Applications*. Springer, 2010, pp. 340–347.

[8] A. Israr, S. Zhao, K. Schwalje, R. Klatzky, and J. Lehman, "Feel effects: enriching storytelling with haptic feedback," *ACM Transactions on Applied Perception (TAP)*, vol. 11, no. 3, p. 11, 2014.

[9] F. Arafsha, K. M. Alam, and A. El Saddik, "Emojacket: Consumer centric wearable affective jacket to enhance emotional immersion," in *IEEE International Conference on Innovations in Information Technology (IIT)*, 2012, pp. 350–355.

[10] L. A. Jones, M. Nakamura, and B. Lockyer, "Development of a tactile vest," in *Haptic Interfaces for Virtual Environment and Teleoperator Systems, 2004. HAPTICS'04. Proceedings. 12th International Symposium on*, 2004, pp. 82–89.

[11] J. Van Erp, C. Jansen, T. Dobbins, and H. Van Veen, "Vibrotactile waypoint navigation at sea and in the air: two case studies," in *Proceedings of EuroHaptics*, 2004, pp. 166–173.

[12] S. W. Wu, R. E. Fan, C. R. Wottawa, E. G. Fowler, J. W. Bisley, W. S. Grundfest, and M. O. Culjat, "Torso-based tactile feedback system for patients with balance disorders," in *IEEE Haptics Symposium*, 2010, pp. 359–362.

[13] R. E. Fan, C. Wottawa, A. Mulgaonkar, R. J. Boryk, T. C. Sander, M. P. Wyatt, E. Dutson, W. S. Grundfest, and M. O. Culjat, "Pilot testing of a haptic feedback rehabilitation system on a lower-limb amputee," in *IEEE International Conference on Complex Medical Engineering*, 2009, pp. 1–4.

[14] P. Kapur, S. Premakumar, S. A. Jax, L. J. Buxbaum, A. M. Dawson, and K. J. Kuchenbecker, "Vibrotactile feedback system for intuitive upper-limb rehabilitation," in *IEEE World Haptics*, 2009, pp. 621–622.

[15] M. F. Rotella, K. Guerin, X. He, and A. M. Okamura, "HAPI bands: a haptic augmented posture interface," in *IEEE Haptics Symposium*, 2012, pp. 163–170.

[16] S. Kulkarni, C. J. Fisher, P. Lefler, A. Desai, S. Chakravarthy, E. Pardyjak, M. A. Minor, and J. M. Hollerbach, "A full-body steerable wind display for a locomotion interface," *IEEE Transactions on Visualization and Computer Graphics*, vol. 21, pp. 1146–1159, 2015.

[17] J. Miehlbradt, A. Cherpillod, S. Mintchev, M. Coscia, F. Artoni, D. Floreano, and S. Micera, "Data-driven body–machine interface for the accurate control of drones," *Proceedings of the National Academy of Sciences*, p. 201718648, 2018.

[18] C. Rognon, S. Mintchev, F. Dell'Agnola, A. Cherpillod, D. Atienza, and D. Floreano, "Flyjacket: An upper body soft exoskeleton for immersive drone control," *IEEE Robotics and Automation Letters*, vol. 3, no. 3, pp. 2362–2369, 2018.

[19] K. O. Johnson, "The roles and functions of cutaneous mechanoreceptors," *Current Opinion in Neurobiology*, vol. 11, no. 4, pp. 455–461, 2001.

[20] G. Ambrosi, A. Bicchi, D. D. Rossi, and E. Scilingo, "The role of contact area spread rate in haptic discrimination of softness," in *IEEE International Conference on Robotics and Automation*, 1999, pp. 305–310.

[21] E. Coevoet, T. Morales-Bieze, F. Largilliere, Z. Zhang, M. Thieffry, M. Sanz-Lopez, B. Carrez, D. Marchal, O. Goury, J. Dequidt *et al.*, "Software toolkit for modeling, simulation, and control of soft robots," *Advanced Robotics*, vol. 31, no. 22, pp. 1208–1224, 2017.